

Determination of the titanium spectral function from $(e, e'p)$ data

L. Jiang,¹ A. M. Ankowski,² D. Abrams,³ L. Gu,¹ B. Aljawrneh,⁴ S. Alsalmi,⁵ J. Bane,⁶ A. Batz,⁷ S. Barcus,⁷ M. Barroso,⁸ V. Bellini,⁹ O. Benhar,¹⁰ J. Bericic,¹¹ D. Biswas,¹² A. Camsonne,¹¹ J. Castellanos,¹³ J.-P. Chen,¹¹ M. E. Christy,¹¹ K. Craycraft,⁶ R. Cruz-Torres,¹⁴ H. Dai,¹ D. Day,³ A. Dirican,¹⁵ S.-C. Dusa,¹¹ E. Fuchey,¹⁶ T. Gautam,¹² C. Giusti,¹⁷ J. Gomez,^{11,*} C. Gu,¹⁸ T. J. Hague,¹⁹ J.-O. Hansen,¹¹ F. Hauenstein,²⁰ D. W. Higinbotham,¹¹ C. Hyde,²⁰ Z. Jerzyk,²¹ A. M. Johnson,²² C. Keppel,¹¹ C. Lanham,¹ S. Li,²³ R. Lindgren,³ H. Liu,²⁴ C. Mariani,^{1,†} R. E. McClellan,¹¹ D. Meekins,¹¹ R. Michaels,¹¹ M. Mihovilovic,²⁵ M. Murphy,¹ D. Nguyen,³ M. Nycz,¹⁹ L. Ou,¹⁴ B. Pandey,¹² V. Pandey,^{1,‡} K. Park,¹¹ G. Perera,³ A. J. R. Puckett,¹⁶ S. N. Santiesteban,²³ S. Širca,^{26,25} T. Su,¹⁹ L. Tang,^{11,12} Y. Tian,²⁷ N. Ton,³ B. Wojtsekhowski,¹¹ S. Wood,¹¹ Z. Ye,²⁸ and J. Zhang³

(The Jefferson Lab Hall A Collaboration)

¹Center for Neutrino Physics, Virginia Tech, Blacksburg, Virginia 24061, USA

²SLAC National Accelerator Laboratory, Stanford University, Menlo Park, California 94025, USA

³Department of Physics, University of Virginia, Charlottesville, Virginia 22904, USA

⁴North Carolina Agricultural and Technical State University, Greensboro, North Carolina 27401, USA

⁵King Saud University, Riyadh 11451, Kingdom of Saudi Arabia

⁶The University of Tennessee, Knoxville, Tennessee 37996, USA

⁷The College of William and Mary, Williamsburg, Virginia 23187, USA

⁸Georgia Institute of Technology, Georgia 30332, USA

⁹INFN, Sezione di Catania, Catania, 95123, Italy

¹⁰INFN and Dipartimento di Fisica, Sapienza Università di Roma, I-00185 Roma, Italy

¹¹Thomas Jefferson National Accelerator Facility, Newport News, Virginia 23606, USA

¹²Hampton University, Hampton, Virginia 23669, USA

¹³Florida International University, Miami, Florida 33181, USA

¹⁴Massachusetts Institute of Technology, Cambridge, Massachusetts 02139, USA

¹⁵Department of Physics, University of Maryland, College Park, Maryland 20742, USA

¹⁶University of Connecticut, Storrs, Connecticut 06269, USA

¹⁷Dipartimento di Fisica, Università degli Studi di Pavia and INFN, Sezione di Pavia, I-27100 Pavia, Italy

¹⁸Duke University, Durham, North Carolina 27708, USA

¹⁹Kent State University, Kent, Ohio 44242, USA

²⁰Old Dominion University, Norfolk, Virginia 23529, USA

²¹Department of Physics, St. Norbert College, De Pere, Wisconsin 54115, USA

²²Department of Physics, Gettysburg College, Gettysburg, Pennsylvania 17325, USA

²³University of New Hampshire, Durham, New Hampshire 03824, USA

²⁴Columbia University, New York, New York 10027, USA

²⁵Jozef Stefan Institute, Ljubljana 1000, Slovenia

²⁶Faculty of Mathematics and Physics, University of Ljubljana, Ljubljana 1000, Slovenia

²⁷Shandong University, Shandong, 250000, China

²⁸Physics Division, Argonne National Laboratory, Argonne, Illinois 60439, USA

The E12-14-012 experiment, performed in Jefferson Lab Hall A, has measured the $(e, e'p)$ cross section in parallel kinematics using a natural titanium target. Here, we report the full results of the analysis of the data set corresponding to beam energy 2.2 GeV, and spanning the missing momentum and missing energy range $15 \lesssim p_m \lesssim 300$ MeV/c and $12 \lesssim E_m \lesssim 80$ MeV. The reduced cross section has been measured with $\sim 7\%$ accuracy as function of both missing momentum and missing energy. We compared our data to the results of a Monte Carlo simulations performed using a model spectral function and including the effects of final state interactions. The overall agreement between data and simulations is quite good ($\chi^2/\text{d.o.f.} = 0.9$).

Introduction: The recent measurement of the $^{40}_{18}\text{Ar}(e, e'p)$ cross section—performed by the E12-14-012 collaboration in Jefferson Lab Hall A—has enabled the first determination of the spectral function describing the

joint energy-momentum distribution of protons in the target nucleus [1].

The JLab experiment, while also providing valuable new information on single-nucleon dynamics in complex nuclei, was primarily meant to obtain the input needed to improve the interpretation of data collected by neutrino experiments using liquid argon detectors, thus reducing the systematic uncertainty of neutrino energy reconstruction.

In principle, the extension of the analysis based on nu-

* deceased

† mariani@vt.edu

‡ Present Address: Department of Physics, University of Florida, Gainesville, FL 32611, USA

clear spectral functions to both neutrino and antineutrino interactions would require the availability of the neutron energy-momentum distribution in argon, whose experimental study using electron beams involves challenging issues.

The analysis of the data collected by a pioneering ${}^4\text{He}(e, e'n)$ experiment, carried out at NIKHEF in the 1990s [2], has clearly demonstrated that—in contrast to the case of the $(e, e'p)$ reaction—neutron knockout involves additional difficulties, associated with both the detection of the outgoing neutron and a reliable identification of the reaction mechanism. A comparison between the results of theoretical calculations and the measured cross section, corresponding to momentum transfer $q = 300$ MeV/ c and missing momentum in the range $25 < p_{\text{miss}} < 70$ MeV/ c , shows that in this kinematic regime charge-exchange processes—in which the detected neutron is *not* produced at the elementary interaction vertex—provide the dominant contribution, and must be carefully taken into account.

An alternative, admittedly rather crude, procedure to obtain information on the neutron distribution in argon is based on the observation that the neutron spectrum of ${}^{40}_{18}\text{Ar}$ is mirrored by the proton spectrum of the nucleus of titanium, having charge $Z = 22$. Based on this property, which reflects the isospin symmetry of nuclear forces, it has been argued that the proton spectral function obtained from $\text{Ti}(e, e'p)$ data provides a viable proxy for the neutron spectral function of argon [3]. The validity of this hypothesis is supported by the results of Ref. [4], whose authors have employed the proton and neutron spectral functions of argon obtained from a state-of-the-art theoretical model to carry out an accurate calculation of the double-differential ${}^{40}_{18}\text{Ar}(\nu_\mu, \mu^-)$ cross section. The results obtained replacing the neutron spectral function of argon with the proton spectral function of titanium turn out to be in remarkably good agreement; in fact, they are nearly indistinguishable from one another.

In this letter, we report the results of the analysis of the $\text{Ti}(e, e'p)$ data collected in Jefferson Lab Hall A by the E12-14-012 collaboration, and discuss the representation of the reduced cross sections in terms of a model proton spectral function.

Experimental setup: Experiment E12-14-012 was approved by the Jefferson Lab PAC in 2014 and data was taken in the Spring 2017. In the past few years a series of measurements have been completed: the inclusive, (e, e') [3, 5, 6], and exclusive $(e, e'p)$ [1, 7] electron scattering cross sections on several targets, including a natural gas argon target [1, 7].

An electron beam of 2.2 GeV and ≈ 22 μA was provided by the Jefferson Lab Continuous Electron Beam Accelerator Facility (CEBAF). The scattered protons and electrons were detected in coincidence in two nearly identical high-resolution spectrometers (HRSS) both consisting of a dipole and three quadrupole magnets. The electron and proton spectrometers are both equipped with vertical drift chambers (VDCs) [8], scintillator

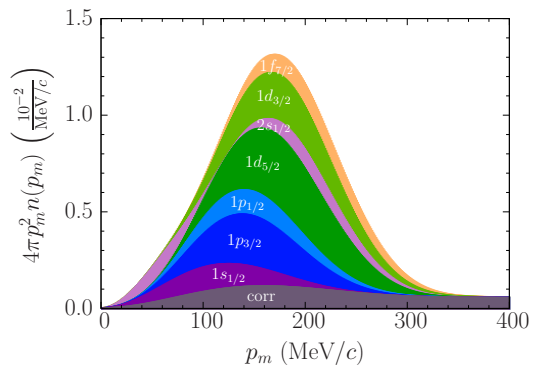


FIG. 1. Missing momentum distribution of protons in titanium in the test spectral function, presented with the geometric factor of $4\pi p_m^2$.

TABLE I. Parametrization of the test spectral function of protons in titanium. For each shell-model state α , we compare the occupation number in the independent particle shell-model N_α with the assumed spectroscopic factor S_α . The peak of the missing energy distribution E_α of the width σ_α is also provided. For the correlated part, we give its total normalization and the threshold for two-nucleon knockout E_{thr} .

α	N_α	S_α	E_α (MeV)	σ_α (MeV)
$1f_{7/2}$	2	1.6	11.45	2
$1d_{3/2}$	4	3.2	12.21	2
$2s_{1/2}$	2	1.6	12.84	2
$1d_{5/2}$	6	4.8	15.46	4
$1p_{1/2}$	2	1.6	35.0	6
$1p_{3/2}$	4	3.2	40.0	6
$1s_{1/2}$	2	1.6	62.0	10
corr.	—	4.4	22.09	—

planes (two) for timing measurements and triggering, and a double-layered lead-glass calorimeter. In addition, the electron arm is equipped with a gas Čerenkov counter for particle identification and pion rejectors, while the proton arm is equipped with pre-shower and shower detectors [9]. The experimental kinematics used during data taking on the natural titanium target were very similar to the those used for the Ar target [1].

The six-fold differential cross section as a function of p_m and E_m was extracted from the data using the $(e, e'p)$ event yield Y for each p_m and E_m bin as described in Ref. [1].

The reduced cross section was obtained as a function of p_m and E_m , from the double differential cross section using the elementary electron-proton off-shell cross section σ_{ep} of de Forest [10, 11].

The JLab SIMC spectrometer package [12] was used to simulate $(e, e'p)$ events as described in detail in Ref. [1]. Simulation included an approximate spectral function for Ti, geometric details of the target, radiative corrections, and Coulomb effects.

The simulated momentum distributions are presented in Fig. 1.

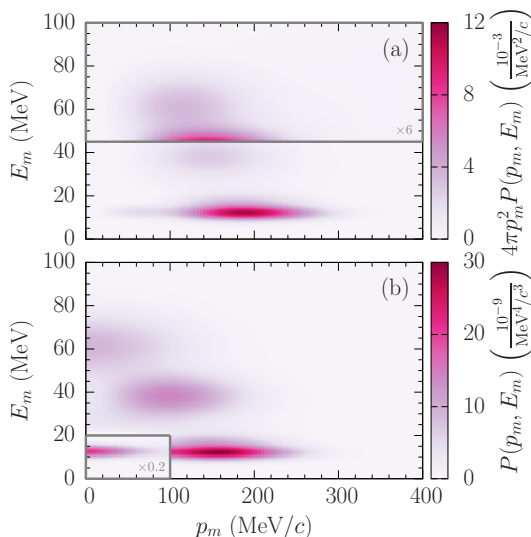


FIG. 2. Test spectral function shown (a) with and (b) without the geometric factor of $4\pi p_m^2$. Note that multiplicative factors are used for clearer presentation of some regions.

TABLE II. Contributions to systematic uncertainties for titanium averaged over all the E_m and p_m bins for each kinematics. All numbers are in %. For kin4, the results correspond to the systematic uncertainties of the signal and the background added in quadrature.

	kin1	kin2	kin3	kin4
1. Total statistical uncertainty	0.78	0.60	0.82	1.24
2. Total systematic uncertainty	4.63	4.92	4.70	6.04
a. Beam $x&y$ and HRS offset	0.75	1.71	1.19	1.47
b. Optics (q1, q2, q3)	0.48	0.77	0.55	0.90
c. Acceptance cut (θ, ϕ, z)	1.36	1.46	1.32	1.57
d. Target thickness/density/length	0.20	0.20	0.20	0.20
e. Calorimeter & Čerenkov & β cuts	0.29	0.58	0.42	2.83
f. Radiative and Coulomb corr.	1.00	1.00	1.00	1.00
g. Cross section model and FSI	4.12	2.23	2.23	2.23
h. Trigger and coincidence time cut	0.78	0.33	0.58	2.32

The missing energy of the shell-model states is assumed to follow the Gaussian distribution as in Ref. [1]. The correlated spectral function is determined following the approach described in Ref. [1]. By construction, the correlated part accounts for 20% of the total strength of the test spectral function, see Table I.

Figure 2 displays the test spectral function as a function of missing momentum and missing energy.

Data Analysis: The total systematic uncertainty in this analysis is the sum in quadrature of the individual uncertainties as listed in Table II. We followed the same procedure as described in Ref. [1]: kinematic and acceptance cuts are considered uncorrelated bin to bin and they do not depend on the theoretical input model. All the kinematic and acceptance cuts were varied according to the variable's resolution. The simulation did not

contain correction for final state interaction (FSI) effects other than the transparency corrections. We repeated the analysis of systematic uncertainties varying all MC input parameters, and did not observe any substantial variations of the obtained results. To determine the uncertainties related to the target position, we performed the simulation with the inputs for the beam's and spectrometer's x and y offsets varied within uncertainties, and we recomputed each time the optical transport matrix varying the three quadrupole magnetic fields, one at the time. Each of these runs was compared to the reference run, and the corresponding differences were summed in quadrature to give the total systematic uncertainty due to the Monte Carlo simulation as described in Ref. [1, 7].

We set our E_m ranges, 0 to 30 MeV, 30 to 54 MeV, and 54 to 90 MeV. We performed the fit of the missing momentum distribution using the three contributions associated with the three missing energy regions to improve our sensitivity.

We have performed a fit to the experimental missing energy and missing momentum distributions to extract spectroscopic factors, mean value and width of each of the ^{48}Ti orbitals, as detailed in Ref. [1].

For each bin in the spectra of missing energy (100×1 MeV) and missing momentum (40 bins with momentum range changing between kinematics), we determined the product of the reduced MC cross section [14] and the ratio of the data to simulation yield,

$$\frac{d^2 \sigma_{cc1}^{\text{red}}}{d\Omega dE'} = \left(\frac{d^2 \sigma_{cc1}^{\text{red}}}{d\Omega dE'} \right)_{\text{MC}} \times \frac{Y(E', \theta)}{Y_{\text{MC}}(E', \theta)}, \quad (1)$$

where the $Y(E', \theta)$ is the yield for a given bin and the reduced MC cross section is a fit to the existing data [12]. The reduced cross section includes (i) the σ_{cc1} cross section of de Forest [10], (ii) the predictions of the spectral function model, (iii) radiative corrections [15], (iv) Coulomb corrections [16], and (v) FSI corrections, described within the distorted-wave impulse approximation (DWIA) scheme.

The fit performs a χ^2 minimization using the MINUIT [17] package available in ROOT [18].

The χ^2 function is defined as:

$$\chi^2 = \sum_i \chi_i^2 = \sum_i \left(\frac{\sigma_i^{\text{red, obs}} - \sum_\alpha S_\alpha f_\alpha^{\text{pred}}(i)}{\sigma_{\sigma_i^{\text{red, obs}}}} \right)^2, \quad (2)$$

where the index i labels the missing momentum bin, α is the orbital index, $f_\alpha^{\text{pred}}(i)$ is the parametrized prediction evaluated at bin i in the missing momentum spectra for orbital α , S_α is the spectroscopic factor. The missing momentum distribution does not show dependence on the mean energies and widths of the orbitals.

In the case of the minimization in missing momentum, the results are summarized in Table III, where we report all the fit results with degrees of freedom and the value of the χ^2 . We repeated the fit a second time excluding the correlated SF contribution to understand possible bias

TABLE III. Comparison of the results of the χ^2 minimization using the missing momentum distributions, determined with and without the use of the correlated spectral function. For every state α , we determined the spectroscopic factor S_α , and its occupation number in an independent-particle shell model, N_α . We include the total spectroscopic strength, the number of degrees of freedom (d.o.f.), and the χ^2 per d.o.f.

α	N_α	w/ corr.	w/o corr.
$1f_{7/2}$	2	0.83 ± 1.17	0.78 ± 1.35
$1d_{3/2}$	4	1.17 ± 0.22	1.34 ± 0.10
$2s_{1/2}$	2	2.02 ± 0.08	2.18 ± 0.08
$1d_{5/2}$	6	2.34 ± 1.34	2.34 ± 3.72
$1p_{1/2}$	2	2.46 ± 0.27	2.71 ± 1.19
$1p_{3/2}$	4	5.46 ± 1.69	5.46 ± 0.05
$1s_{1/2}$	2	2.17 ± 0.09	2.51 ± 0.08
corr.	0	5.15 ± 0.41	excluded
$\sum_\alpha S_\alpha$		21.60 ± 2.51	17.32 ± 4.20
d.o.f.		675	676
$\chi^2/\text{d.o.f.}$		0.49	0.57

TABLE IV. External constraints on the fits to the missing-energy spectra computed using data from past measurements [19–22]. For the clarity of presentation, we denote E_α as $E(\alpha)$.

Parameter	Value (MeV)	Uncertainty (MeV)
$E(1f_{7/2})$	11.32	0.10
$E(1d_{3/2})$	12.30	0.24
$E(2s_{1/2})$	12.77	0.25
$E(1d_{5/2})$	15.86	0.20
$E(1d_{5/2}) - E(1d_{3/2})$	3.57	0.31
$E(1p_{3/2}) - E(1p_{1/2})$	6.36	0.75

due to the assumptions used to compute the correlated part of the spectral functions [1].

The spectroscopic factors reported in Tables III and V are normalized to $80\% \times 22$ for the total strength of the orbitals and to $20\% \times 22$ for the correlated part and they include corrections due to phase space coverage.

We then repeat the fit minimizing the χ^2 function using the missing energy spectra,

$$\chi^2 = \sum_i \chi_i^2 + \sum_n \left(\frac{\tau_n^{\text{fit}} - \tau_n^c}{\sigma_n^{\text{fit}}} \right)^2. \quad (3)$$

We include constraints on the position of the topmost energy levels from previous experimental results [19–22], summarized in Table IV as penalty terms in our χ^2 function [1].

The spin-orbit splitting has been computed using the phenomenological prescription of Ref. [21, 22], $E(n, l, l - 1/2) - E(n, l, l + 1/2) = \frac{2l+1}{2n} kA^{-C}$, with angular momentum l , main quantum number n , and mass number A . The empirically determined constants $k = 23.27$ MeV and $C = 0.583$ [21] are included in the fit as penalty function to the χ^2 . The uncertainty value has been cal-

TABLE V. Results of the χ^2 minimization using the missing energy distributions, obtained with and without using all priors, with and without the use of the results from the missing-momentum fits, and excluding the correlated part of the spectral function. For every state α , we show the extracted spectroscopic factor S_α , and its occupation number in the independent-particle shell model, N_α . Additionally, we provide the total spectroscopic strength, the number of degrees of freedom (d.o.f.), and the χ^2 per d.o.f.

α	N_α	all priors	w/o p_m	w/o corr.
$1f_{7/2}$	2	1.53 ± 0.25	1.55 ± 0.28	1.24 ± 0.22
$1d_{3/2}$	4	2.79 ± 0.37	3.15 ± 0.54	3.21 ± 0.37
$2s_{1/2}$	2	2.00 ± 0.11	1.78 ± 0.46	2.03 ± 0.11
$1d_{5/2}$	6	2.25 ± 0.16	2.34 ± 0.19	3.57 ± 0.29
$1p_{1/2}$	2	2.00 ± 0.20	1.80 ± 0.27	2.09 ± 0.19
$1p_{3/2}$	4	2.90 ± 0.20	2.92 ± 0.20	4.07 ± 0.15
$1s_{1/2}$	2	2.14 ± 0.10	2.56 ± 0.30	2.14 ± 0.11
corr.	0	4.71 ± 0.31	4.21 ± 0.46	excluded
$\sum_\alpha S_\alpha$		20.32 ± 0.65	20.30 ± 1.03	18.33 ± 0.59
d.o.f.		121	153	125
$\chi^2/\text{d.o.f.}$		0.95	0.71	1.23

TABLE VI. Measured peak positions E_α , widths σ_α , and the parameter E_{corr} of the correlated spectral function obtained from the minimization of χ^2 using the missing energy distributions. We compare the results with and without constraints coming from the missing momentum fit.

α	E_α (MeV)		σ_α (MeV)	
	w/ priors	w/o priors	w/ priors	w/o priors
$1f_{7/2}$	11.32 ± 0.10	11.31 ± 0.10	8.00 ± 5.57	8.00 ± 6.50
$1d_{3/2}$	12.30 ± 0.24	12.33 ± 0.24	7.00 ± 0.61	7.00 ± 3.84
$2s_{1/2}$	12.77 ± 0.25	12.76 ± 0.25	7.00 ± 3.76	7.00 ± 3.84
$1d_{5/2}$	15.86 ± 0.20	15.91 ± 0.22	2.17 ± 0.27	2.23 ± 0.29
$1p_{1/2}$	33.33 ± 0.60	33.15 ± 0.65	3.17 ± 0.45	3.03 ± 0.48
$1p_{3/2}$	39.69 ± 0.62	39.43 ± 0.68	5.52 ± 0.70	5.59 ± 0.70
$1s_{1/2}$	53.84 ± 1.86	52.00 ± 3.13	11.63 ± 1.90	13.63 ± 2.59
corr.	25.20 ± 0.02	25.00 ± 0.29	—	—

culated comparing the prediction of the phenomenological prescription to the available experimental data from NIKHEF-K [23–25].

The missing energy spectra minimization returns 23 parameters in total: 3 parameters for each orbital (the spectroscopic factor, the position of the maximum, and the width of the distribution) and 2 parameters for the correlated SF (the strength and the threshold energy).

We present our results in Table V. We repeated the fit excluding the results coming from the p_m minimization and without the correlated SF part. All the results are compatible within errors, which indicates no large bias in the determination of the spectroscopic factors using different set of constraints.

We have also repeated the minimizations using different sets of priors for the orbital parametrizations: the Maxwell-Boltzmann or Gaussian distributions, with the

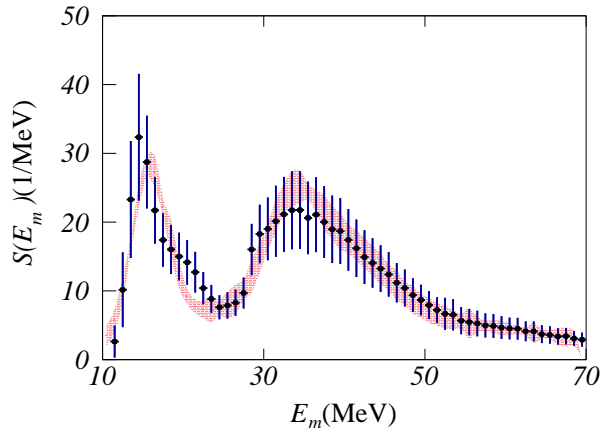


FIG. 3. Missing energy distributions obtained for natural titanium for $130 < p_m < 260$ MeV/c. The red band indicates the final fit results including the full error uncertainties.

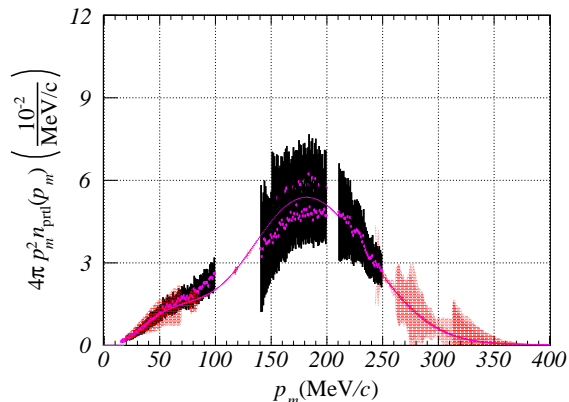


FIG. 4. Partial momentum distribution obtained by integrating the test spectral function over the missing energy range of 0–30 MeV presented with the geometric factor of $4\pi p_m^2$. Different data regions represent data from different kinematics.

width governed by a constant or linearly dependent on the distance from the Fermi energy, $E_m - E_F$. The results obtained are all compatible within errors, which indicates that the fit is relatively independent of the parametrization used.

The results of Fig. 3 show that the test spectral function model, rescaled using the parameters obtained from the fit, listed in Table V, is capable to reproduce our data satisfactorily. The SF parametrization obtained from the fit is represented by the red band, which accounts for the full error budget, including correlations and FSI correction uncertainties.

Figure 4 reports the missing momentum distribution obtained integrating the data and the model over the missing energy range 30–54 MeV.

It is apparent that the collected data cover the relevant kinematic range with just a few exceptions, most

notably at vanishing p_m . The experimental coverage is not complete due to experimental conditions and beam-time limitation. In particular, data for kinematics 4 is statistically limited.

A remarkable feature of Fig. 4 is the agreement—within admittedly sizable uncertainties—of the reduced cross sections corresponding to kinematics 2 and 3. As observed in Ref. [1], this agreement supports the validity of the DWIA treatment of FSI, and, more generally, of the factorisation scheme underlying our analysis.

Summary and conclusions: The Ti($e, e'p$) data collected by experiment E12-14-012 at Jefferson Lab have been analysed to obtain the target spectral function, describing the energy and momentum distribution of protons bound in the titanium ground state. The model dependence involved in the determination of the spectral function is mainly arising from the treatment of FSI, and the associated uncertainties, that have been included in the analysis as described in Ref. [1, 7].

The results of our study of titanium provide important novel information, critical to the interpretation of events observed in liquid argon detectors when the primary interaction involves a neutron of the Ar nucleus. The results of the pioneering work of Barbieri *et al.* [4] demonstrate that a replacement of the neutron SF of argon with the proton SF of ^{48}Ti in the calculation of the $^{40}\text{Ar}(\nu_\mu, \mu^-)$ cross section at beam energy $E_\nu = 1$ GeV has a few-percent effect. It has to be kept in mind, however, that the inclusive cross section, which only involves integrals of the SFs, is rather insensitive to the details of the missing energy distributions. Therefore, the findings of Barbieri *et al.*, while being very encouraging, cannot be taken as clear-cut evidence of the validity of the assumption that the proton SF of natural titanium can be used as a proxy for the neutron SF of Ar, as suggested by isospin symmetry. More work will be necessary to put this hypothesis on a firm basis.

The reduced differential cross sections has been fitted using a model spectral function. The effects of FSI, which are known to be significant in ($e, e'p$) reactions, have been included using the same factorization scheme which underlines our analysis and, as for the case of Ar [1], seems to be reliable.

The comparison between data and MC simulation results has been showed in a broad range of missing energies, extending from the proton-knockout threshold to $E_m \sim 80$ MeV. The overall agreement, supports the validity of the theoretical basis of our analysis.

We have determined the position and width of the peaks corresponding to shell model states, and estimated the corresponding spectroscopic strengths.

A more accurate determination of the titanium spectral function will require a more advanced theoretical model of the energy and momentum distributions, as well as a refined implementation of the DWIA.

The extraction of the spectral function reported in this article—providing a satisfactory description of the proton energy and momentum distribution—should be seen as

the achievement of the goals of the JLab experiment E12-14-012, and a step toward a more accurate description of (anti)neutrino interactions in argon.

The understanding of the proton and neutron spectral functions for argon will greatly improve the accuracy of neutrino and antineutrino energy reconstruction in measurements of neutrino oscillations, such as those in the short-baseline program of Fermilab and in the long-baseline studies in the Deep Underground Neutrino Experiment. The spectral function, being an intrinsic property of the target nucleus, is relevant to the description of all reaction channels, including quasielastic scattering, resonance production, and deep-inelastic scattering [26].

ACKNOWLEDGMENTS

We acknowledge the outstanding support from the Jefferson Lab Hall A technical staff, target group and Ac-

celerator Division. This experiment was made possible by Virginia Tech, the National Science Foundation under CAREER grant No. PHY-1352106 and grant No. PHY-1757087, PHY-480915 and PHY-2149165. This work was also supported by the DOE Office of Science, Office of Nuclear Physics, contract DE-AC05-06OR23177, under which Jefferson Science Associates, LLC operates JLab, DOE contract DE-FG02-96ER40950, DE-AC02-76SF00515, DE-SC0013615 and by the DOE Office of High Energy Physics, contract DE-SC0020262.

-
- [1] L. Jiang *et al.* (Jefferson Lab Hall A Collaboration), Phys. Rev. D **105**, 112002 (2022).
 - [2] A. Misiejuk *et al.*, Phys. Rev. Lett. **89**, 172501 (2002).
 - [3] H. Dai, *et al.* (Jefferson Lab Hall A Collaboration), Phys. Rev. C **98**, 014617 (2018).
 - [4] C. Barbieri, N. Rocco, and V. Somà, Phys. Rev. C **100**, 062501 (2019).
 - [5] H. Dai *et al.* (Jefferson Lab Hall A Collaboration), Phys. Rev. C **99**, 054608 (2019).
 - [6] M. Murphy *et al.* (Jefferson Lab Hall A Collaboration), Phys. Rev. C **100**, 054606 (2019).
 - [7] L. Gu *et al.* (Jefferson Lab Hall A Collaboration), Phys. Rev. C **103**, 034604 (2021).
 - [8] K. G. Fissum *et al.*, Nucl. Instrum. Methods Phys. Res. A **474**, 108 (2001).
 - [9] J. Alcorn *et al.*, Nucl. Instrum. Methods Phys. Res. A **522**, 294 (2004).
 - [10] T. de Forest Jr., Nucl. Phys. A **392**, 232 (1983).
 - [11] A. E. L. Dieperink, T. de Forest Jr., I. Sick, and R. A. Brandenburg, Phys. Lett. B **63**, 261 (1976).
 - [12] SIMC Monte Carlo, https://hallcweb.jlab.org/wiki/index.php/SIMC_Monte_Carlo.
 - [13] T. Nikšić, N. Paar, D. Vretenar, and P. Ring, Comput. Phys. Commun. **185**, 1808 (2014).
 - [14] J. Arrington *et al.*, Phys. Rev. Lett. **82**, 2056 (1999).
 - [15] L. W. Mo and Y. S. Tsai, Rev. Mod. Phys. **41**, 205 (1969).
 - [16] A. Aste, C. von Arx, and D. Trautmann, Eur. Phys. J. A **26**, 167 (2005).
 - [17] F. James, “MINUIT Function Minimization and Error Analysis: Reference Manual Version 94.1,” CERN-D-506.
 - [18] R. Brun and F. Rademakers, Nucl. Instrum Methods Phys. Res. A **389**, 81 (1997).
 - [19] Meng Wang, G. Audi, F. G. Kondev, W. J. Huang, S. Naimi, and Xing Xu, Chin. Phys. C **41**, 030003 (2017).
 - [20] J. Chen, Nucl. Data Sheets **149**, 1 (2018).
 - [21] G. Mairle, M. Seeger, H. Reinhardt, T. Kihm, K. T. Knöpfle, and Chen Lin Wen, Nucl. Phys. A **565**, 543 (1993).
 - [22] G. Mairle, Phys. Lett. B **304**, 39 (1993).
 - [23] G. J. Kramer *et al.*, Phys. Lett. B **227**, 199 (1989).
 - [24] M. Leuschner *et al.*, Phys. Rev. C **49**, 955 (1994).
 - [25] G. J. Kramer, The proton spectral function of ^{40}Ca and ^{48}Ca studied with the $(e, e'p)$ reaction. An investigation of ground-state correlations, Ph.D. thesis, University of Amsterdam, 1990.
 - [26] E. Vagnoni, O. Benhar, and D. Meloni, Phys. Rev. Lett. **118**, 142502 (2017).